# A novel finite-difference time-domain approach to the self-consistent simulation of high-speed TW-EAMs

F. Cappelluti, F. Bertazzi, G. Ghione

Dipartimento di Elettronica, Politecnico di Torino, Torino, Italy, fcappell@athena.polito.it

**We present a novel self-consistent time-domain model for the analysis and design of traveling-wave electroabsorption modulators (TW-EAMs). The model fully accounts for the nonlinear interaction between the microwave and optical traveling fields. The effects on the bandwidth and modulation efficiency of the nonuniform optical field distribution along the device are discussed. A few examples of application are presented, showing the model to be an efficient tool for the analysis, design and optimization of TW-EAMs for analog and digital applications.**

## INTRODUCTION

Traveling-wave electroabsorption modulators are attractive components for both analog and digital high-speed fiber optic links, due to their potential for low on-off voltage, broad band operation. Being fabricated on heavily doped substrates, TW-EAMs exhibit high microwave losses, strongly asynchronous coupling to the optical signal, and impedance mismatch with respect to 50 $\Omega$. Moreover, several nonlinear effects take place in TW-EAMs, affecting the microwave and optical fields propagation as well as their interaction. Firstly, the optical absorption coefficient is a nonlinear function of the applied voltage, and exhibits saturation. Also, the current photogenerated in the active region causes non-uniform microwave losses and saturates at high optical power levels owing to space-charge effects. Finally, the propagation characteristics of the microwave electrodes depend on the applied voltage, owing to the effect of the photocurrent itself and, to a lesser extent, to the nonlinear junction capacitance. The models proposed so far for these devices are usually derived in quasi-static conditions [1] and exploit linear approximations of both the microwave and optical parameters. On the other hand, self-consistent dynamic large-signal modeling is important for gaining insight into microwave and optical power induced saturation mechanisms, modeling harmonics and intermodulation products generation (analog applications), and performing device design and optimization in large-signal operation (OTDM and WDM applications). A time-domain distributed model for the device analysis in the nonlinear electro-optical conversion regime may be found in [2]. However, the microwave line is treated as linear and no feedback exists between the microwave and optical line, i.e. the microwave line works in low-power conditions and the effects of photocurrent and of nonuniform bias along the modulator are neglected.

In the present paper, we introduce a novel self-consistent dynamic approach which enables to model the nonlinear distributed interaction between the optical and microwave signals. A circuit-oriented large-signal model has been developed for the microwave structure, treated as a nonlinear quasi-TEM transmission line with optical power dependent propagation characteristics. The optical field behavior is studied by solving the wave equation in presence of a time/spatial variation of the complex optical refractive index, induced by the electrical modulating field. Self-consistency is required since the absorbed optical power, locally dependent on the microwave field, drives the carriers generation, and the parameters of the electrical model are, in turn, photocurrent dependent.

As an example, we investigate the behaviour of a typical InGaAsP/InP TW-EAM in small-signal (SS) and large-signal (LS) operation. Its performance in terms of bandwidth, linearity and chirp are investigated as examples of application. Simulation results under high-speed digital modulation are also presented. The technique is validated in SS and low optical power condition through a comparison with the results of the SS frequency-domain approach in [1].

## THE DISTRIBUTED TIME-DOMAIN MODEL

The equivalent electric circuit of the per-unit-length TW-EAM cross-section is depicted in Fig. 1. In this circuit, $L$ and $C$ are the inductance and capacitance of the unloaded microwave electrode, while $Z_{\mathrm{con}}(f)$ models the frequency-dependent conductor impedance. The EA section is modeled through the device series resistance $R_{\mathrm{S}}$, representing the resistivity of $p$ and $n$ semiconductor layers and metal contacts, the $p$-$i$-$n$ junction capacitance $C_{\mathrm{j}}\left(v_{\mathrm{j}}\right)$, and the photocurrent generator $I_{\mathrm{ph}}\left(v_{\mathrm{j}}, P_{\mathrm{op}}\right)$, which provides the coupling between the optical and microwave transmission lines. The quantities $v_{\mathrm{j}}\left(z,t\right)$ and $P_{\mathrm{op}}\left(z,t\right)$ are the junction voltage and the optical power, respectively.

The per-unit-length TW-EAM model can be derived according to several approximations of increasing complexity. As a first step, the series impedance and parallel admittance can be derived from a quasi-TEM or full-wave EM model; however, this implies that the free charge distribution in the modulator cross section be known. A suitable approximation consists in assuming that the intrinsic absorption layer is depleted and that doped layers have a free carrier distribution equal to doping. This model is accurate enough in linear operation but of course does not include nonlinear effects associated to the junction capacitance. A second-order electromagnetic model, which is under

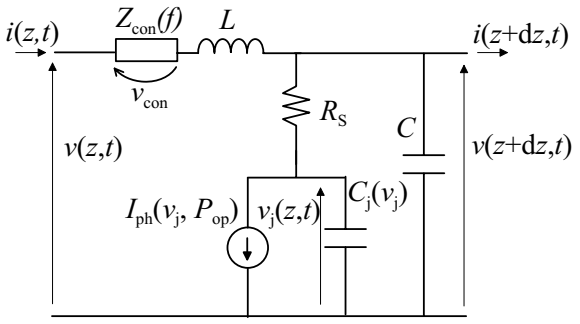


Figure 1: RF equivalent circuit model for the per-unit-length microwave transmission line (MTL).

development, self-consistently solves, in quasi-static conditions, the transport semiconductor equations together with the Poisson equations in DC and small-signal operation thus providing the parallel line per-unit-length parameters as a function of the working point. Standard circuit-oriented procedure can be then implemented to derive a nonlinear per-unit-length model. As already outlined, another major source of nonlinear and dispersive behaviour is provided by the photocurrent itself. Again, saturation mechanisms in the photocurrent due to space-charge effects affecting photocarrier collection can be in principle simulated through the solution of the transport equation in the presence of a suitable optical generation term. Saturation involving the absorption coefficient, on the other hand, is more difficult to model and would require a completely self-consistent quantum model; however, the saturation behaviour of $\alpha$ can be empirically introduced in the semiconductor model thus allowing a full self-consistent simulation of the microwave line as a function of the optical and microwave input powers. Concerning the optical waveguide model, neglecting reflections at the end facets of the modulator, the time-dependent traveling-wave equation which describes the forward-propagating optical wave is derived from Maxwell's equations by exploiting the slowly-varying envelope approximation and treating the electric field induced variations of the optical complex refractive index as a small perturbation. In order to simulate the voltage and optical power dependence of the optical complex refractive index, we use analytical expressions derived by curve fitting either from experimental data or from physics-based simulations of the active region structure.

Assuming the optical power is known, the equivalent circuit in Fig. 1 can be described by two traveling-wave equations and a time-dependent local equation in the variables $v_F$, $v_R$ and $v_j$, where $v_F$, $v_R$ are the forward and reverse voltage propagating along the line, respectively. The dependence of $Z_{\text{con}}$ on frequency is simulated through an infinite impulse response (IIR) digital filter. Boundary and initial conditions are set according to generator and load terminations, and applied bias, respectively. The microwave and optical traveling-wave equations are numerically solved by following a finite-difference approach: the device is

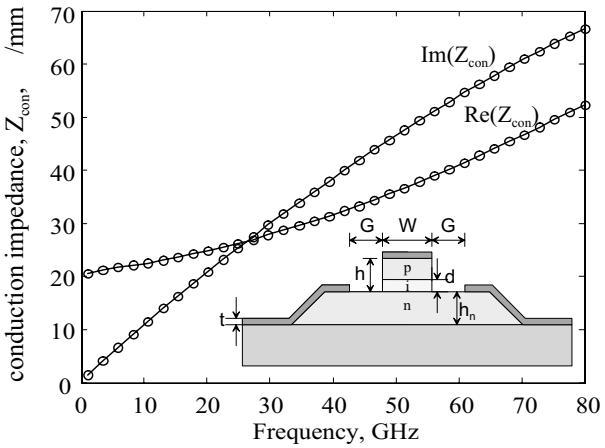


Figure 2: Conduction impedance versus frequency, computed with FEM (solid lines) and simulated through the discrete-time IIR filter (circles).

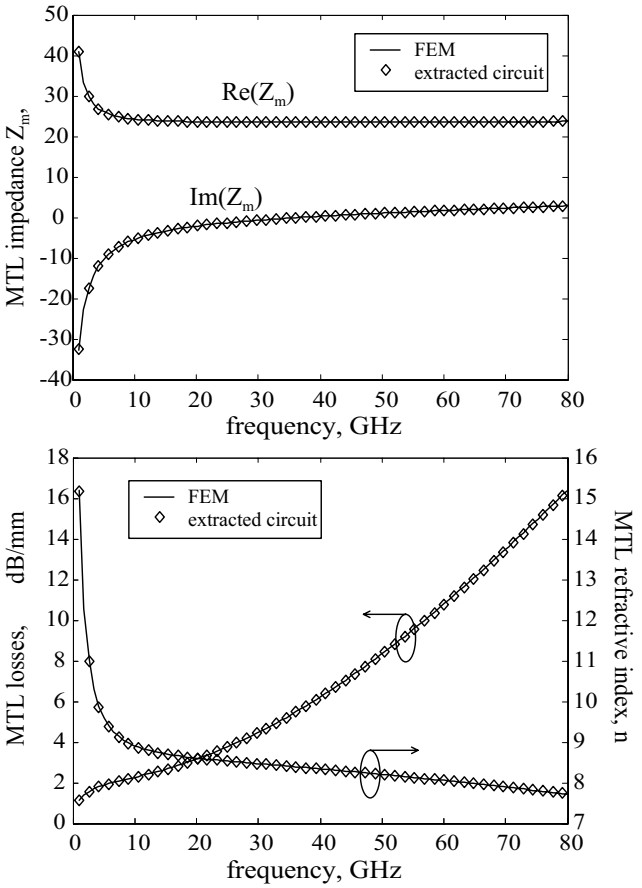


Figure 3: MTL characteristic impedance (above) and microwave complex propagation constant (below) computed from full-wave FEM analysis and from the extracted MTL equivalent circuit.

longitudinally divided into an integer number of small sections having equal length $\Delta z = v_f \Delta t$. The resulting numerical system is solved through a time-stepped ($\Delta t \ll R_{\text{S}} C_{\text{j}}$) iterative approach. To account for the velocity mismatch between the optical and electrical signals, two different spatial grids are used for the optical and microwave signals.

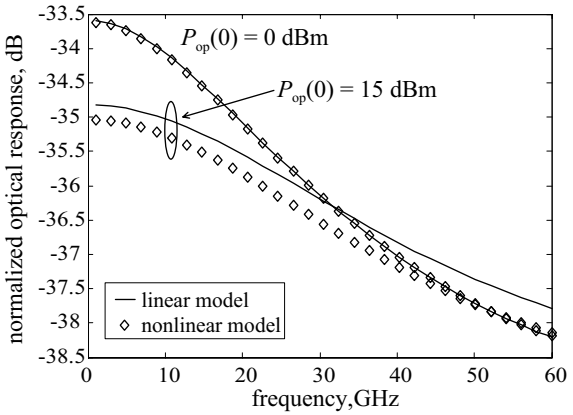


Figure 4: Small signal optical response, at different incident optical powers, predicted by the linear (-) and non linear (symbol) model. The optical response is normalized to the input optical power.

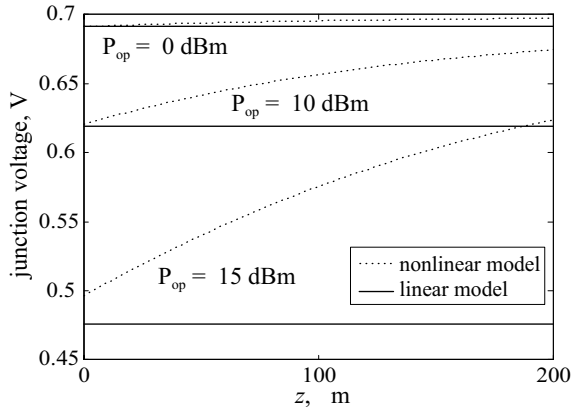


Figure 5: Junction voltage variation along the device, at different optical power levels, predicted by the linear (continuous) and nonlinear (dashed) model.

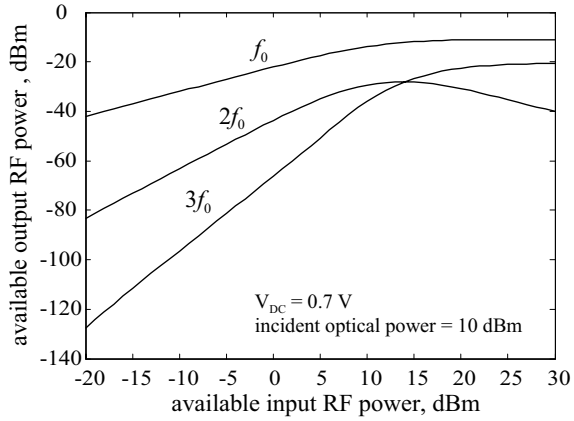


Figure 6: RF harmonics generation and saturation effect under single-tone RF input signal.

## RESULTS

We consider the MQW InGaAsP/InP EAM sketched in the inset of Fig. 2. The microwave structure of the device is a coplanar waveguide (the gold electrode thickness is $t = 1\ \mu$m, the central electrode width is $W = 3\ \mu$m, and the line-to-ground spacing is $G = 10\ \mu$m) on a ridge-type semiconductor substrate (the ridge-height is $h = 2\ \mu$m). The n-type and intrinsic layer thickness are $h_n = 2\ \mu$m, $d = 0.3\ \mu$m, respectively. The device length is 200 $\mu$m. The microwave propagation characteristics, for low optical power, have been computed via an accurate full-wave finite element (FEM) approach [3]. The intrinsic layer was assumed to be completely depleted. The per-unit-length MTL equivalent circuit has been fitted to the simulated MTL impedance and complex propagation constant (Fig. 3), with excellent agreement. The extracted circuit parameters are: $C = 0.094$ pF/mm, $L = 0.53$ nH/mm, $R_s = 0.82\ \Omega$mm, and $C_j = 1.15$ pF/mm. A third order rational polynomial has been used to fit the frequency behavior of $Z_{\rm con}(f)$. As for the optical parameters of the active layer, that is the change of absorption coefficient and refractive index with applied bias, we have used the experimental data reported in [4]. The optical confinement factor in the active layer is $\Gamma_{\rm o} = 0.2$, while the residual absorption $\alpha_0$ has been set to 15 dB/mm, which is a typical value for EAMs. An optical group index of 3.5 has been used. An empirical model has been adopted for the optical power induced saturation of the absorption coefficient. Concerning SS analysis, under low optical power illumination ($0\mathrm{dBm}$), the simulation results are compared against the linear approach proposed in [1], obtaining the excellent agreement shown in Fig. 4. Note that the SS uniform model in [1] can be easily derived from the equivalent circuit in Fig. 1 by assuming uniform bias along the MTL and approximating the time-domain photocurrent generator as an optical power dependent resistor $R_0 = (dI_{ph}/dv_j)^{-1}$, evaluated at the junction bias. However, as the optical power increases the linear model results to be less accurate, since it cannot account for non-uniform microwave losses and non-uniform EAM bias voltage that occur at higher optical power (Fig. 5).

In order to demonstrate the effectiveness of our numerical approach, a linearity analysis of the modulator has been performed under single-tone excitation ($f_0 = 1$ GHz), as a function of the RF input power (Fig. 6) as well as of the incident optical power (Fig. 7). The RF amplitude modulation curves were extracted from the computed time-domain output optical waveforms through a Fast Fourier Transform (FFT). The responsivity and impedance of the receiver were set to 0.8 A/W and 50 $\Omega$, respectively. At high optical power levels (see Fig. 7), the deviation of the curves slope from the SS value 2 is due to the "self-biasing" of the device (see Fig. 5), which leads to a locally varying modulation efficiency (in terms of $\partial\alpha/\partial v_{\rm j}$). In (Fig. 8) and (Fig. 9) the modulator frequency chirping is evaluated in SS and LS operation, respectively. The "static chirp" in Fig. 8 refers to the chirp parameter, $\alpha_{\rm H}$, directly computed from the optical properties of the active material as a function of the applied bias. Notice that a strong dependence of $\alpha_{\rm H}$ on the applied bias $V_{DC}$ is observed. The same qualitative behavior is found in LS operation:

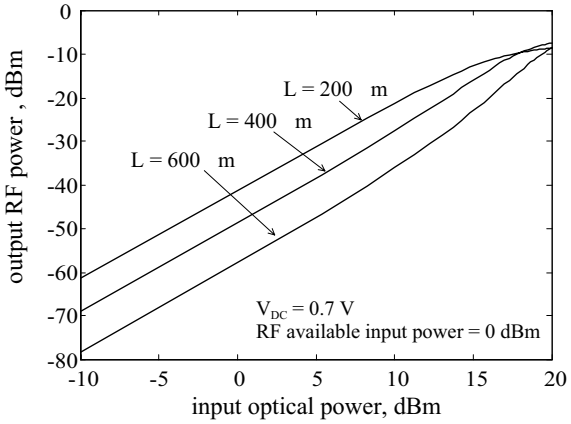


Figure 7: Optical power induced saturation for different device lengths.

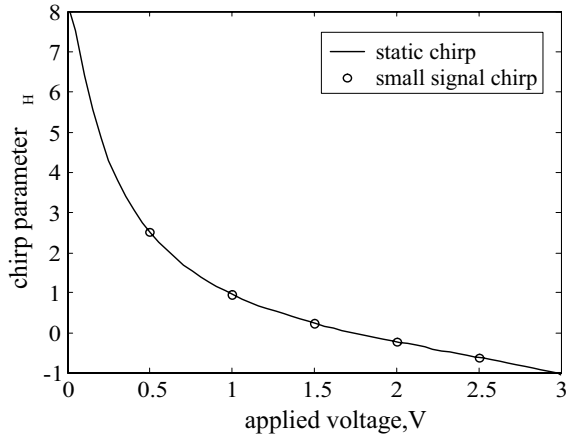


Figure 8: Chirp parameter $\alpha_{\mathrm{H}}$ versus applied voltage for the optical parameters in [4].

at $V_{\mathrm{DC}} = 1,\ 1.5$ V the chirp is positive, with positive frequency shift on the leading-edge of the optical intensity, and negative frequency shift on the trailing-edge, whereas at $V_{\mathrm{DC}} = 2,\ 2.5$ V negative chirp occurs, reversing the positions of the frequency components with respect to the optical wave edges. As last example, the voltage applied to the modulator was modulated by a NRZ 64 random bit pattern from 0 V to 4 V, at the rate of 10 and 40 Gbps, and successively filtered by a RC filter with time constant of 10 ps (10 Gbps) and 2.5 ps (40 Gbps). The calculated optical eye diagrams at the output of the modulator, with 10 dBm incident optical power, are shown in Fig. 10.

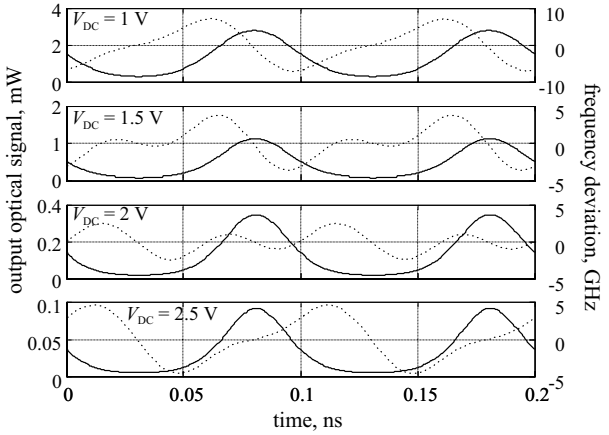


Figure 9: Time-resolved frequency chirp in large signal operation, at different bias voltages. Solid lines: optical intensity; dashed lines: frequency shift.

## CONCLUSIONS

A novel finite-difference time-domain approach to the self-consistent, dynamic simulation of traveling-wave electroabsorption modulators has been presented, together with a few examples of application in small- and large-signal operation.

## ACKNOWLEDGEMENTS

This research has been partially funded by the Center of Excellence on Multimedia RadioCOmmunications (CERCOM) of Politecnico di Torino, under the project line WP-2.

## REFERENCES

[1] G.L. Li et al., *IEEE Trans. Microwave Theory Techn.*, Vol. 47, No. 7, Part: 2, pp. 1177–1183, 1999.

[2] Y.J. Chiu et al., *IEEE Photon. Technol. Lett.*, Vol. 13, No. 8, pp. 791–793, 2001.

[3] F. Bertazzi et al., *IEEE Trans. Microwave Theory Techn.*, Vol. 50, No. 9, 2002

[4] L. M. Zhang et al.,*IEEE J. Quantum Electron.*, Vol. 30, No. 11, pp. 2573–2577, 1994.

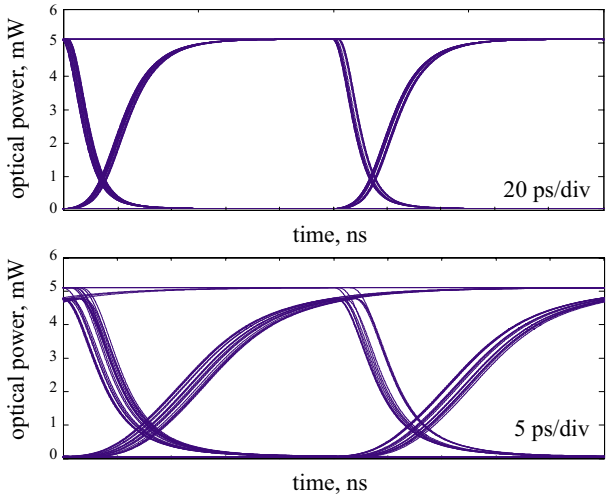


Figure 10: Calculated optical eye diagrams under 64 bit NRZ modulation at the rate of 10 Gbps (above) and 40 Gbps (below).